



Local loss model of dividing flow in a bifurcate tunnel with a small angle^{*}

Xin ZHANG^{1,3}, Tian-hang ZHANG^{1,2}, Yun-ge HOU^{1,2}, Kai ZHU^{1,4}, Zhi-yi HUANG^{1,2}, Ke WU^{†1,2}

¹College of Civil Engineering and Architecture, Zhejiang University, Hangzhou 310058, China

²Key Laboratory of Offshore Geotechnics and Material of Zhejiang Province, Hangzhou 310058, China

³School of Electronic Engineering, Xi'an Shiyou University, Xi'an 710065, China

⁴College of Quality and Safety Engineering, China Jiliang University, Hangzhou 310018, China

[†]E-mail: wuke@zju.edu.cn

Received May 13, 2018; Revision accepted Nov. 16, 2018; Crosschecked Dec. 25, 2018

Abstract: To provide a theoretical basis for the flow diversion control of a bifurcate tunnel, the flow separation characteristics and local loss model at the tunnel bifurcation were analyzed by combining numerical simulation and theoretical derivation. The results showed that the sudden change of boundaries interrupts uniform flow when air flows through a tunnel bifurcation, causing changes in flow velocity and direction. When the diversion ratio β is small, the flow is separated on the downstream mainline tunnel sidewall close to the bifurcation point and the ramp sidewall away from bifurcation point; when β is large, the flow is separated on the downstream mainline sidewall away from bifurcation point and the ramp sidewall close to bifurcation point. The local loss on flow division is caused mainly by velocity gradient changes and flow deflection and separation. When the air flux ratio q of the downstream mainline tunnel to that of the ramp is equal to their cross-sectional area ratio ϕ , local loss coefficients are at their minimum; when $q > \phi$, the loss coefficients decrease with the increase of β , but the loss coefficient for the ramp increases as the bifurcation angle rises. When $q < \phi$, the loss coefficients increase with the increase of β , but the loss coefficient for the ramp declines as the bifurcation angle rises. Finally, a theoretical formula to predict the dividing flow local loss coefficient of a bifurcate tunnel is established based on the airflow deflection angle assumption. The proposed model has a higher precision in prediction than other formulas.

Key words: Bifurcate tunnel; Dividing flow; Local loss mechanism; Flow separation characteristics; Computational fluid dynamics (CFD); Theoretical formula

<https://doi.org/10.1631/jzus.A1800298>

CLC number: TH113

1 Introduction

Tunnels are an important construction applied in urban areas to relieve traffic congestion (Li et al., 2012; Du et al., 2015). As urban tunnels are always located in

downtown areas, more and more tunnels are designed with multiple on/off-ramps to connect with ground road networks to provide multiple access points (Meng et al., 2011; Tan and Gao, 2015). These connections serve important districts along the alignment and form a 3D transportation system. Such a branching design will inevitably divert the air flux and its contaminants, thus changing their distribution inside the tunnel and directly affecting the environment inside and outside the tunnel (Li et al., 2015). The key to effective flow diversion control and ventilation design of bifurcate tunnels is to understand the air flow characteristics and local loss features at the tunnel bifurcation.

[‡] Corresponding author

^{*} Project supported by the Natural Science Foundation of Zhejiang Province (No. LY19E080028), the Key Research and Development Project of Zhejiang Province (No. 2018C03029), and the Fundamental Research Funds for the Central Universities (No. 2017QNA4023), China

 ORCID: Xin ZHANG, <https://orcid.org/0000-0002-1613-7082>; Ke WU, <https://orcid.org/0000-0003-2313-3124>

© Zhejiang University and Springer-Verlag GmbH Germany, part of Springer Nature 2019

Studies of the flow characteristics and local loss features of bifurcate tunnels are quite rare. Structurally, a bifurcate tunnel is similar to a bifurcate pipeline. When air flows through the tunnel bifurcation, the sudden change of the tunnel shape causes changes in the velocity, direction and distribution of the flow, the air changing from approximately 1D flow to 3D flow. During the change of flow pattern, intense friction and momentum exchange occur among fluid particles, causing local energy loss (Hager, 2010; Abdulwahhab et al., 2013). Li et al. (2001) conducted numerical and experimental studies on the flow process of fluid in a bifurcate pipe with an angle of 64° and discovered that changes in the flow direction and velocity distribution due to centrifugal force were the main causes of local losses at the bifurcation. Based on potential flow theory, Iwanami et al. (2008) analyzed the flow field features and pressure loss mechanism in a bifurcate pipeline with an angle of 90° . They showed that, after the bifurcation, pressure loss in the main pipe was similar to that in a sudden enlargement, whereas the pressure loss in the lateral pipe was modeled as the sum of the loss in a contraction followed by a sudden enlargement. Ghostine et al. (2013), Mignot et al. (2013), and Momplot et al. (2017) focused on the flow structures in an open-channel bifurcation with an angle of 90° . They found that, by means of the aspect ratio and Froude number in the upstream channel, the occurrence of each branch of recirculation can be predicted.

Multiple factors affect local loss in a bifurcate structure, including the area ratio, flow ratio, angle between two branches, Reynolds number (Re), chamfer, and the cross-sectional shape of the channel (Miller, 1971; Idelchik et al., 2008). Usually, when $Re < 1.5 \times 10^5$, the local loss coefficient tends to decrease with the increase of Re . When $Re \geq 1.5 \times 10^5$, the flow enters a region of quadratic resistance law, where the local loss coefficient does not vary with Re and depends only on the form of the bifurcate structure (Shi et al., 2013). An experiment was conducted to investigate the effect of the type of chamfer at the intersection of two branches. Results indicated that, compared to a sharp chamfer, a rounded chamfer can enhance the turbulence along the lateral pipe, allow momentum to diffuse more efficiently, and reduce the area of the backflow zone, thereby lowering the local loss coefficient of the lateral pipe (Costa et al., 2006; Lukiyanto et al., 2016). A large radius of curvature of

a rounded chamfer is associated with a low local loss coefficient. The local loss coefficient of the main pipe is almost unaffected by the type of chamfer (Itō and Imai, 1973). The flow ratio and the angle between two branches have more significant effects on the local loss coefficient than the cross-sectional shape (Miller, 1971). Through a lot of experimentation, Idelchik et al. (2008) found that when the angle between two branches fell within the range of 45° – 120° , the local loss coefficient and flow ratio can be related by a second-order parabolic equation. Hager (1984), Bassett et al. (2001), and Oka and Itō (2005) derived a theoretical formula based on the laws of conservation of mass, energy, and momentum, which could be used to calculate the local loss coefficient for any flow ratio and angle, and could be verified using test data within 45° – 120° . Note that the radius of curvature at the intersection of the mainline tunnel and the ramp should not be too small, to ensure smooth traffic flow at the intersection and improve safety and ride comfort along the linear transition section (from the ramp nose to the starting point of the design speed control curve of the ramp) (MOT, 2018). Therefore, many bifurcate tunnels with a small bifurcation angle exist. For instance, the Zizhi Tunnel in Hangzhou, China has a bifurcation angle of 10.2° on the No. 1 west-line and 7.4° on the No. 3 east-line. The Chinese Qingdao Jiaozhou Bay subsea tunnel has a bifurcation angle of 5° . However, the angle of a bifurcate structure appearing in most of the literature about the characteristics of dividing flow and local loss is equal to or greater than 45° . Thus, the applicability of the existing formula to small angles is doubtful due to the lack of verification studies of local loss coefficients of small angles.

Adopting the method of computational fluid dynamics (CFD), in this paper we build a 3D mathematical model of air motion in a bifurcate tunnel, and analyze the dividing flow characteristics and local loss features in the bifurcate structure with an angle range of 5° to 15° to determine the relationships between the dividing flow local loss coefficient and the flow ratio and bifurcation angle. Based on the flow separation mechanism, we also propose a theoretical formula for the dividing flow local loss coefficient of a bifurcate tunnel for design purposes. The present findings can improve tunnel ventilation design theory and provide a theoretical basis for the flow diversion control of bifurcate tunnels.

2 Mathematical model

2.1 Governing equations

The air flow in tunnels during ventilation is assumed to be a steady incompressible flow with constant viscosity and density and is usually turbulent (Nan et al., 2015). The flow process follows the fundamental laws of physics, i.e. the laws of conservation of mass and momentum. In this paper, the Reynolds-averaged Navier–Stokes equations (RANS equations) (Versteeg and Malalasekera, 1995; Liao et al., 2018) are primarily used to describe turbulent flows. RANS equations are time-averaged equations of motion for fluid flow. The idea behind the equations is Reynolds decomposition, whereby an instantaneous quantity is decomposed into its time-averaged and fluctuating quantities, an idea first proposed by Reynolds (1895). The governing equation can be written in the Cartesian coordinate system as follows:

$$\frac{\partial u_i}{\partial x_i} = 0, \quad (1)$$

$$\frac{\partial}{\partial x_j}(\rho u_i u_j) = -\frac{\partial P}{\partial x_i} + \frac{\partial}{\partial x_j} \left(\mu \frac{\partial u_i}{\partial x_j} - \rho \overline{u'_i u'_j} \right) + S_i, \quad (2)$$

where x_i is the coordinate components, u_i is the time-averaged velocity component, and u'_i is the fluctuating component, $i, j=1, 2, 3$; $\overline{\rho u'_i u'_j}$ is the Reynolds stress; ρ , μ , and P are the mass density of air, turbulent viscosity, and static pressure, respectively; S_i is the generalized source term.

These equations can be used with approximations based on the knowledge of properties of flow turbulence to give approximate time-averaged solutions to the Navier–Stokes equations. Yet, RANS equations are highly non-linear, with a greater number of independent variables than the number of dimensions of the system. To close the equation system, this study adopts the Realizable k - ε turbulence model, which is able to simulate diversion, reflow, and rotation (Shih et al., 1995). The generated term of the turbulent kinetic energy caused by buoyancy and the expansion and dissipation terms ascribed to the compressibility of the fluid are not taken into account. The transport equations of the turbulent kinetic en-

ergy k and turbulent dissipation rate ε in the Realizable k - ε turbulence model are shown in Eqs. (3) and (4).

$$\frac{\partial(\rho u_i)}{\partial x_i} = \frac{\partial}{\partial x_j} \left[\left(\mu + \frac{\mu_t}{\sigma_k} \right) \frac{\partial k}{\partial x_j} \right] + G_k - \rho \varepsilon, \quad (3)$$

$$\frac{\partial(\rho \varepsilon u_i)}{\partial x_i} = \frac{\partial}{\partial x_j} \left[\left(\mu + \frac{\mu_t}{\sigma_\varepsilon} \right) \frac{\partial \varepsilon}{\partial x_j} \right] + \rho C_1 E \varepsilon - \rho C_2 \frac{\varepsilon^2}{k + \sqrt{\nu \varepsilon}}, \quad (4)$$

where ν is the coefficient of kinematic viscosity; G_k refers to the generated term of the turbulent kinetic energy caused by the mean velocity gradient; E stands for the strain rate; $\mu_t = \rho C_\mu k^2 / \varepsilon$, is the turbulent viscosity. The model coefficients C_μ , C_1 , C_2 , σ_k , and σ_ε are determined by the principle of gradualism which proposes that simple flow results predicted by the model should be consistent with those from direct numerical simulation or experimentation. This has been discussed in detail in the literature. Here, the coefficients C_μ and C_1 are not constant (for the formula, please refer to Tavoularis and Corrsin (1981) and Shih et al. (1994)); the coefficients σ_k , σ_ε , and C_2 are equal to 1.0, 1.2, and 1.9, respectively (Mohamed and Larue, 1990; Shih et al., 1995). Lin and Ferng (2016) reported that taking the model coefficients as above would be satisfactory for solving many fluid flow problems, including the flow in a tunnel.

The Realizable k - ε model as a turbulence model for high Re numbers is not applicable to the near-wall area where the flowing Re number is low. Therefore, the Realizable k - ε model should be used with wall functions. Wall functions are the semi-empirical formula which can relate the physical quantities on the wall with the solution variables in the turbulent core area with high Re numbers. Because of their capability to partly account for the effects of pressure gradients, the non-equilibrium wall functions are recommended for use in complex flows involving separation, reattachment, and impingement where the mean flow and turbulence are subjected to pressure gradients and rapid changes (Nazif and Tabrizi, 2011). Thus, non-equilibrium wall functions were selected to be used with the Realizable k - ε model in this study.

2.2 Numerical algorithm

The finite volume method is used to discretize the governing equations. For the discretization of derivatives, the skewness-corrected linear upwind interpolation scheme (second-order accuracy) is applied to the convective terms, and the second-order linear interpolation is used with a non-orthogonal correction scheme for diffusive terms (Hong et al., 2017). The solution of the velocity field and pressure field is conducted through a fully coupled block algorithm. Due to the simultaneous solution of momentum and continuity equations, implicit block coupling of pressure and velocity variables leads to a faster convergence than with conventional loosely coupled and segregated algorithms of the semi-implicit method for pressure linked equations (SIMPLE) family of algorithms (Mangani et al., 2014).

2.3 Model description and boundary conditions

The mock object is a bifurcate tunnel with an off-ramp with a rectangular cross-sectional shape. The upstream mainline tunnel, the downstream mainline tunnel, and the ramp are a three-lane highway, a two-lane highway, and a one-lane highway with corresponding cross-sectional dimensions of 13.55 m×7 m, 9.75 m×7 m, and 7.55 m×7 m, respectively. Three bifurcation angles, namely 5°, 10°, and 15° are considered separately. The whole domain is meshed by non-uniform hexahedral grids. Due to the application of wall functions, it is not necessary to refine the grids in the near-wall domain. Instead, only the near-wall node should be arranged in the log-law regions of a turbulent wall layer. That is, the y^+ value should be distributed between 30 and 300. y^+ is defined as a dimensionless parameter of distance which can be used to describe the flow in the viscous sublayer and log-law layer. The expression is as follows:

$$y^+ = \frac{u^* y}{\nu}, \quad (5)$$

where u^* refers to the friction velocity near the wall, and y refers to the distance of the near-wall node to the solid surface.

According to y^+ , the distance of the near-wall node to the solid surface is calculated, which is also

corrected continuously through computational simulation. Ultimately, it can be determined that y^+ can be ensured to be between 33 and 280 under all computation conditions when the first layer grid thickness is 0.02402 m.

The tunnel entrance adopts the Dirichlet boundary condition, with an air velocity directly given. The mainline tunnel and ramp exits adopt the Neumann boundary conditions with outflow. The tunnel walls and pavement are taken as impenetrable and non-slip boundaries.

2.4 Grid dependence study

Grid density has a tremendous impact on the numerical simulation results. When the grid number is relatively small, the dispersion error will be quite large; when the grid number is large, not only does the rounding error increase, but also the calculation quantity. Fig. 1 shows the velocity profile of the downstream mainline tunnel 0.8 m away from the bifurcation surface under different grid orders of 1.2×10^5 , 4.3×10^5 , 2.32×10^6 , and 8.01×10^6 . The number of grids greatly influences the velocity profile. When the number of grids reaches 2.32×10^6 , the velocity profile no longer changes with increasing grid number. Therefore, the grid density of this number was adopted in this study.

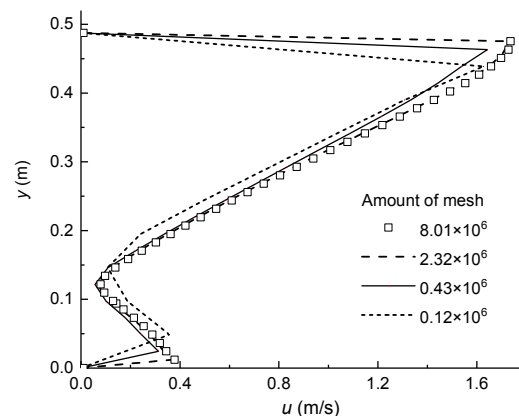


Fig. 1 Velocity profile at different mesh resolutions

2.5 Validation

The mathematical model was validated by the test results of a reduced scale tunnel (Wu et al., 2017) with a length of 29.46 m and a cross-sectional scaling ratio of 1/20 (Fig. 2). The cross-sections of the

upstream mainline tunnel, the downstream mainline tunnel, and the ramp were rectangular with dimensions of 0.6775 m×0.35 m, 0.4875 m×0.35 m, and 0.3775 m×0.355 m, respectively. The bifurcation angle θ could be adjusted within the range of 5°–30°. To satisfy resistance similarity, the tunnel model was made of galvanized steel sheet with a relative roughness of about 0.00108, which is the same as the relative roughness of the real tunnel. When the air velocity of the model tunnel was greater than 2.5 m/s, it could synchronously meet the similarity criteria for resistance (Re), inertial force (Sr), and pressure (Eu).

In the experiment, $\theta=10^\circ$. The #1 jet fan in the upstream mainline tunnel was opened to ensure the air flow at the start of the model tunnel entered into a region of quadratic resistance law. The jet velocities of the #2 and #3 jet fans located at the downstream mainline tunnel and ramp, respectively, were adjusted to change the diversion ratio β , defined as a ratio between the air flux in the ramp and the air flux in the upstream mainline tunnel, from 0.2 to 0.8. To guarantee data reliability, the selected measuring cross-sections, including 1-1, 2-2, and 3-3, were at a distance of more than 20 times the hydraulic diameter away from the bifurcation surface of the tunnel to ensure that the flow on each measuring cross-section had developed into turbulent flow. When turbulent flow had fully developed in the cross-section the static pressure was evenly distributed, while the mean air velocity u_{ave} of the cross-section was linear with the maximum air velocity u_{max} (McKeon et al., 2004; Song et al., 2016), i.e. $u_{ave}=au_{max}$, in which the compensation coefficients a of the cross-sections 1-1,

2-2, and 3-3 were 0.81, 0.80, and 0.79, respectively. Therefore, the measuring points of the air velocity and the static pressure were located at the center of the cross-section and at a position of $d=0.1$ m, respectively (Fig. 3). The air velocity and pressure data of each measuring point were obtained using a Pitot tube anemometer with precision of ± 0.1 m/s and a Dwyer differential pressure transmitter with precision of ± 0.5 Pa, respectively.

Based on the experimental data, the dividing flow local loss coefficients of the downstream mainline tunnel and ramp, ξ_{12} and ξ_{13} , were obtained according to the definition formula of local loss coefficients (Miller, 1971). The structural size of the numerical model constructed for validation was consistent with that of the scale model, and the relevant mesh density was the same as that stated in Section 3. A comparison of results from the scale test and the numerical simulation is shown in Fig. 4. The CFD simulation results were in accordance with the trend of the experimental data. The maximum relative error was only 6.2%, which indicates that the mathematical

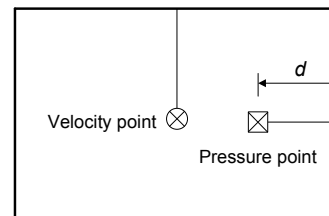


Fig. 3 Arrangement of velocity and pressure measuring points in a cross-section

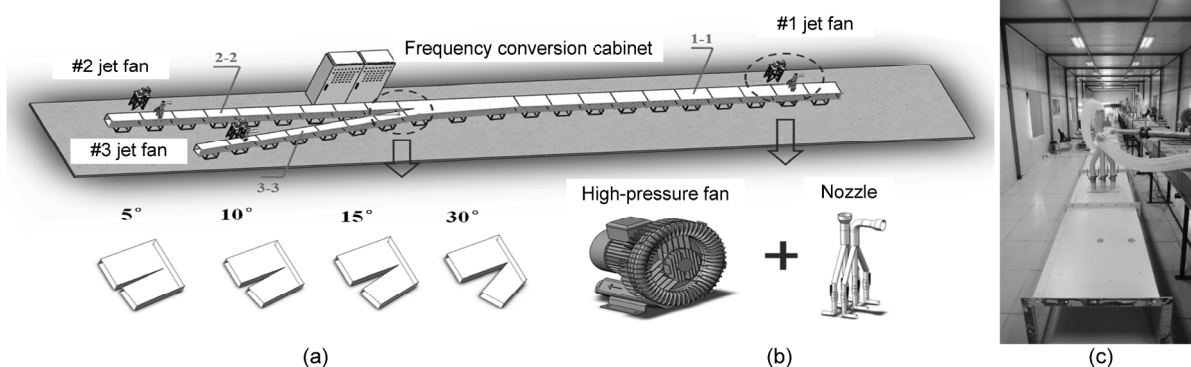


Fig. 2 Schematic diagram of the scale model
(a) Bifurcation section; (b) Jet fan simulator; (c) Realistic scene

model is capable of simulating the local loss for flow division.

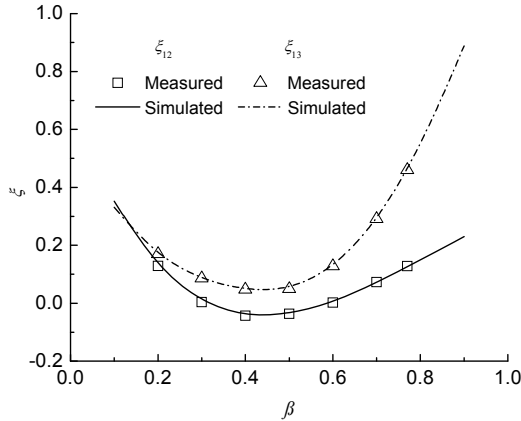


Fig. 4 Comparison of local loss coefficients from simulation and experimental data

3 Results and discussion

3.1 Flow characteristics

When air flows through a tunnel bifurcation the flow is diverted, hence, changing the air flux distribution inside the tunnel. The ratio of the air flux in the downstream mainline tunnel to the air flux in the ramp is denoted as q . Fig. 5 shows the flow field structure at the bifurcation with an angle of 10° under different diversion ratios, β . When β is small, most of the air flows into the downstream mainline tunnel, and the cross-sectional area ratio ϕ (1.3) of the downstream mainline tunnel to the ramp is far smaller than their air flux ratio q (if $\beta=0.1$, $q=9$). Therefore, the velocity of the airflow entering the downstream mainline tunnel will be increased, and a positive velocity gradient will be generated. However, the velocity of the airflow entering the ramp will be decreased, and a negative velocity gradient will be generated. The positive velocity gradient will cause a streamline convergence, while the negative velocity gradient will cause a streamline divergence. As a result, the airflow at the bifurcation will deflect towards the downstream mainline tunnel such that air flowing into it will undergo flow separation on the side wall close to the bifurcation point, while air flowing into the ramp will undergo flow separation on the side wall away from the bifurcation point. The smaller the value of β , the more pronounced will be the flow separation.

As β gradually increases, the air flux in the downstream mainline tunnel declines, while the air flux in the ramp increases so that q gradually approaches ϕ . At this time, the velocity gradient at the bifurcation will be decreased, the streamline will tend to be smooth, and the area of flow separation zone will be reduced. Fig. 4 shows that the local loss coefficient for flow division will decline as β increases during this process. When β has increased to about 0.43, $q \approx 1.3$, and q is equal to ϕ . At this time, the local loss coefficient for flow division will be minimized. Afterwards, with further increases of β , the flow separation zone will gradually enlarge and the local loss coefficient for flow division will increase. However, in this process, the flow field structure will present characteristics obviously different from those found when β is smaller.

Fig. 5 shows that when β is large, most of the air will flow into the ramp, and ϕ will be much larger than q (if $\beta=0.9$, $q=0.1$). At this time, the velocity of the airflow entering the downstream mainline tunnel will be decreased, and a negative velocity gradient will be generated, causing a streamline divergence. However, the velocity of the airflow entering the ramp will be increased, and a positive velocity gradient will be generated, resulting in a streamline convergence. Therefore, airflow at the bifurcation will deflect towards the ramp such that air in the downstream mainline tunnel will undergo flow separation on the side wall away from the bifurcation point. The air in the ramp will undergo flow separation on the side wall close to the bifurcation point. The larger the value of β , the more obvious will be the flow separation.

From the above, it can be seen that as β changes, the mismatch between the downstream mainline tunnel-ramp air flux ratio q and the cross-sectional area ratio ϕ will increase the velocity gradient, the degree of airflow deflection, and the area of the separation zone at bifurcation, thus generating a greater local loss.

Fig. 6 shows the dividing flow local loss coefficients and flow field structure of the bifurcate tunnel at different bifurcation angles, θ . Figs. 6a and 6b show that the airflow deflection and flow separation of the downstream mainline tunnel are almost free from the influence of θ . Thus, variation in the local loss coefficient ξ_{12} with β remains much the same at different values of θ (Fig. 6b).

The airflow deflection and flow separation in the ramp are influenced by both θ and β . Fig. 6a suggests that at a small diversion ratio ($\beta < 0.43$), airflow at the bifurcation will deflect towards the downstream mainline tunnel. Since the airflow deviates from the ramp, the higher the value of θ , the stronger will be the restriction on airflow deflection of the bifurcation structure. Moreover, the more significant the flow

separation near the ramp wall, the larger will be the value of ζ_{13} (Fig. 6c). Fig. 6d reveals that the airflow at the bifurcation will deflect towards the ramp at a large diversion ratio ($\beta > 0.43$). At this point, a larger θ will lead to a better synergy effect between the bifurcation structure and the airflow deflection and separation, and ζ_{13} will be smaller in this case (Fig. 6c).

Consequently, the mismatch between θ and airflow deflection will strengthen the flow separation and increase the local loss in the ramp. This explains why ζ_{13} is generally greater than ζ_{12} at the same β (Fig. 4).

3.2 Local loss coefficients for dividing flow

The sudden change of boundaries interrupts the uniform flow of the fluid when air flows through a tunnel bifurcation, forcing its flow velocity, direction, and distribution to change abruptly. During the change of flow pattern, intense friction and momentum exchange occur among fluid particles, causing local energy loss. Flow field analysis shows that the local losses from flow division are caused mainly by velocity gradient changes and flow deflection and separation. The dividing flow local loss coefficient of the downstream mainline tunnel ζ_{12} is influenced mainly by β , while that of the ramp ζ_{13} is influenced by both θ and β .

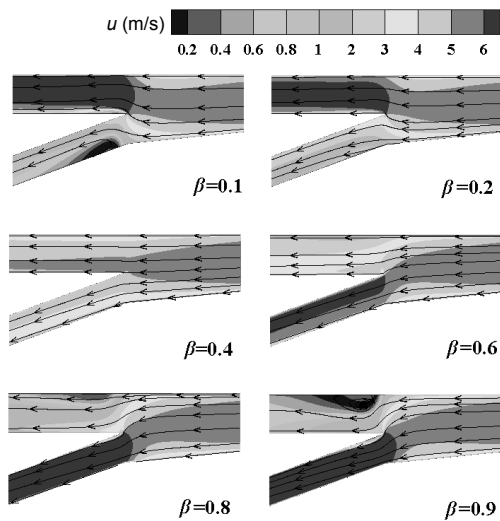


Fig. 5 Flow field structure of the bifurcate tunnel at different values of β

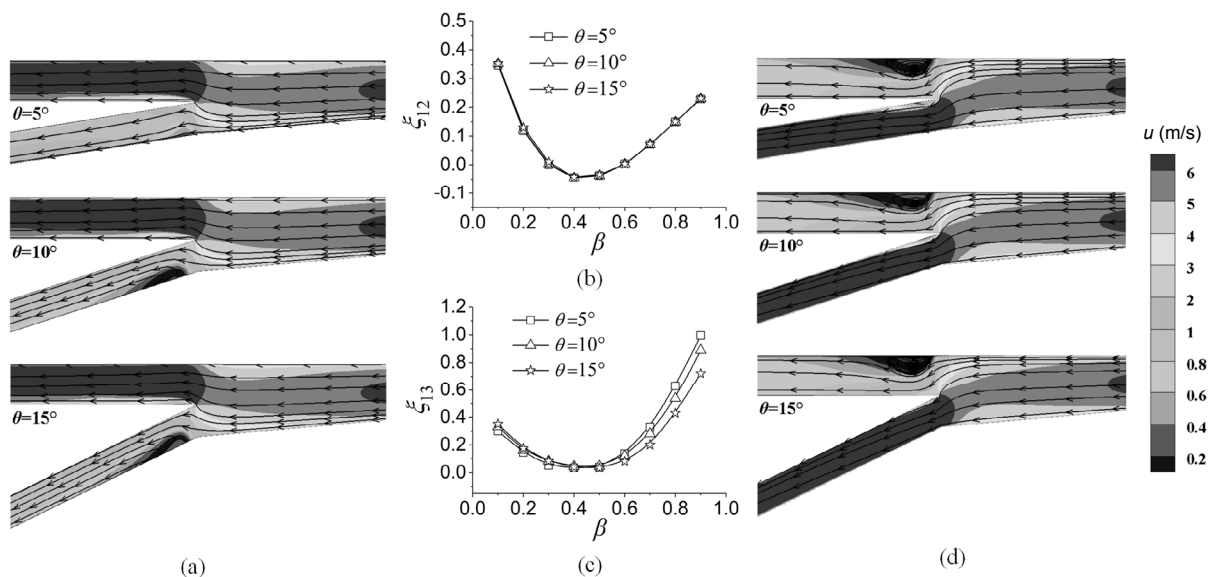


Fig. 6 Local loss coefficients and flow field structure of the bifurcate tunnel with angles of 5° , 10° , and 15°
 (a) Flow structure at $\beta=0.1$; (b) Change law of ζ_{12} ; (c) Change law of ζ_{13} ; (d) Flow structure at $\beta=0.9$

3.2.1 Mainline tunnel

When β is small, the airflow at the bifurcation will deflect towards the downstream mainline tunnel, such that air flowing into the tunnel will undergo flow separation (the region defined by the points $N-M-B$) on the side wall close to the bifurcation point (Fig. 7a). When β is large, the airflow at the bifurcation will deflect towards the ramp, such that air in the downstream mainline tunnel will undergo flow separation on the side wall away from the bifurcation point (Fig. 7b). This separation zone causes a restriction of the flow in the downstream mainline tunnel. The dashed line $M'-M$ represents the points in the mainline tunnel where this restriction is greatest. The free flow area of the downstream mainline tunnel is equal to F_M at this point.

Thus, to evaluate the loss coefficient ξ_{12} , it is necessary to consider two distinct control volumes (Bassett et al., 2001). The first is the region defined by the points $N-N'-M'-M$, denoted region I. The second is bounded by the points $M-M'-B'-B$, denoted region II. Matthew (1975) argued that as flow converges (in region I), the total pressure remains almost constant, and that pressure loss ΔP_B occurs only as the flow encounters a divergence (in region II). Thus, the total pressure of the flow between $N-N'$ and $M-M'$ is assumed to be constant.

The Bernoulli equations for regions I and II, respectively, can be written as

$$P_N + 0.5\rho u_N^2 = P_M + 0.5\rho u_M^2, \quad (6)$$

$$P_M + 0.5\rho u_M^2 = P_B + 0.5\rho u_B^2 + \Delta P_B, \quad (7)$$

where the subscripts N , M , and B represent the cross-sections $N-N'$, $M-M'$, and $B-B'$, respectively. The momentum equation applied respectively to regions I and II, parallel to the mainline, yields

$$P_N F_N - P_M F_M - P_{MN}(F_B - F_M) = \dot{m}_M u_M - \dot{m}_N u_N \cos \gamma, \quad (8)$$

$$P_M F_M + P_{MB}(F_B - F_M) - P_B F_B = \dot{m}_B u_B - \dot{m}_M u_M, \quad (9)$$

where \dot{m} refers to the mass flow rate; F stands for the

cross-sectional area; γ is the deflection angle, i.e. the angle that deviates from the horizontal when the air flows into the downstream mainline tunnel; P_{MN} and P_{MB} are the pressures along the lines $M-N$ and $M-B$, respectively. The term $P_{MN}(F_B - F_M)$ represents the force of static pressure along the line $M-N$ on the control volume I (region I), parallel to the mainline. Hager (1984) argued that the pressure in the separation region can be assumed to be uniform and equal to the static pressure along the line $M-M'$, i.e. $P_{MN} = P_{MB} = P_M$.

Considering the mass flow rates through the cross-sections $M-M'$, $N-N'$, and $B-B'$ are equal, and the cross-sectional areas of sections $N-N'$ and $B-B'$ are the same, i.e. $\dot{m}_M = \dot{m}_N = \dot{m}_B$, $F_N = F_B$, Eqs. (8) and (9) can be rewritten as

$$P_N F_B - P_M F_B = \dot{m}_B u_M - \dot{m}_B u_N \cos \gamma, \quad (10)$$

$$P_M F_B - P_B F_B = \dot{m}_B u_B - \dot{m}_B u_M. \quad (11)$$

By the definition of the mass flow rate, $\dot{m}_B = \rho F_B u_B$, a rearranged expression for ΔP_B can be obtained after combining Eqs. (6), (7), (10), and (11):

$$\Delta P_B = 0.5\rho u_B^2 - \rho u_B u_N \cos \gamma + 0.5\rho u_N^2. \quad (12)$$

According to the definition of the local loss coefficient for flow division, ξ_{12} can be written as

$$\xi_{12} = \frac{\Delta P_B}{0.5\rho u_A^2}, \quad (13)$$

where the subscript A represents the cross-section $A-A'$.

Experiments by Hager (1984) indicated that the velocity of the flow entering the downstream mainline tunnel u_N is approximately equal to u_E , where the subscript E represents the end of the transition section $E'-E''$. According to the conservation of mass, the mass flow rates through sections $A-A'$ and $E'-E''$ are equal, as are the mass flow rates through sections $E'-E$ and $B-B'$. As the flow is incompressible, the application of the mass conservation equations gives

$$u_B = \frac{(1-\beta)F_A}{F_B} u_A, \quad u_E = \frac{F_A}{F_E \cos \delta} u_A, \quad (14)$$

where δ is the deflection angle of the air flowing through the cross-section $E'-E''$. Upon substituting Eqs. (12) and (14) into Eq. (13), Eq. (13) can be rewritten as

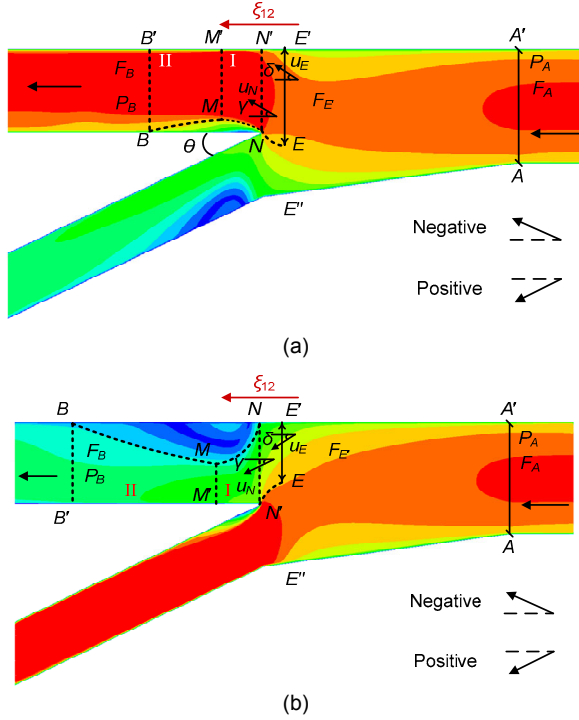


Fig. 7 Control volume used to calculate ξ_{12}
(a) $\beta=0.1$; (b) $\beta=0.9$

$$\xi_{12} = \left(\frac{F_A}{F_B}\right)^2 (1-\beta)^2 - \frac{2F_A^2 \cos \gamma}{F_B F_E \cos \delta} (1-\beta) + \left(\frac{F_A}{F_E \cos \delta}\right)^2 \quad (15)$$

Bassett et al. (2001) indicated that airflow entering the downstream main branch keeps horizontal with the flow direction of the upstream main branch, since the main branches have the same cross-sectional area throughout. However, in a bifurcate tunnel, when the air flows through cross-sections $E'-E''$ and $N-N'$, the flow directions are clearly shifted. The angles of deflection δ and γ are affected by β according to the flow field structure, due to the different sectional areas of the mainline tunnel before and after the diversion. Based on the velocity component data of the cross-section $N-N'$ ($E'-E''$), an inverse trigonometric function is used to calculate the angle of the flow

entering the cross-section $N-N'$ ($E'-E''$) deviating from the horizontal at each grid node. Then, the arithmetic average of those angles is taken as the deflection angle γ (δ). The change rule of δ and γ with β is shown in Fig. 8.

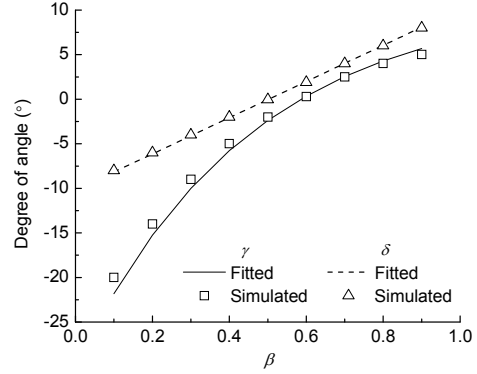


Fig. 8 Change laws of δ and γ with β

With the least square method, the expressions of γ and δ with β can be fitted (the goodness of fit R^2 is 0.99 for both) as follows:

$$\gamma = -41.3e^{-2.2\beta} + 11.4, \quad (16)$$

$$\delta = 20.3\beta - 10.2. \quad (17)$$

Upon substituting Eqs. (16) and (17) into Eq. (15), Eq. (15) can be rewritten as

$$\xi_{12} = \left(\frac{F_A}{F_B}\right)^2 (1-\beta)^2 + \left(\frac{F_A}{F_E \cos(20.3\beta - 10.2)}\right)^2 - \frac{2F_A^2 \cos(-41.3e^{-2.2\beta} + 11.4)}{F_B F_E \cos(20.3\beta - 10.2)} (1-\beta). \quad (18)$$

3.2.2 Ramp

The process for deriving the equation for the dividing flow local loss coefficient of ramp ξ_{13} is analogous to that for the loss coefficient ξ_{12} . The region ($Z-Z'-C'-C$) where the flow separation occurs is taken as the control volume for deriving ξ_{13} , and includes regions III ($Z-Z'-R'-R$) and IV ($R-R'-C'-C$), as shown in Fig. 9. The momentum, Bernoulli's, and mass conservation equations that are parallel to the ramp direction are applied to regions III and IV. After combining and solving, ξ_{13} can be expressed as follows:

$$\xi_{13} = \left(\frac{F_A}{F_C}\right)^2 \beta^2 - \frac{2F_A^2 \cos(\theta - \omega)}{F_C F_E \cos \delta} \beta + \left(\frac{F_A}{F_E \cos \delta}\right)^2, \quad (19)$$

where ω is the deflection angle of the airflow entering the ramp (i.e. flowing through the cross-section Z-Z'). Bassett et al. (2001) considered that the deflection angle of the flow entering the lateral branches is $\theta/4$. However, according to the flow field structure, the deflection angle ω is affected greatly by the changes in θ and β . Based on the CFD simulation results, the change law of ω with β is shown in Fig. 10, under different values of θ . The process of obtaining the value of ω is analogous to that of obtaining the value of γ . With the least square method, the expression of ω can be fitted (the goodness of fit R^2 is 0.99) as follows:

$$\omega = 37.3\beta^{1.8} - 0.4\theta + 5.3. \quad (20)$$

Upon substituting Eqs. (20) and (17) into Eq. (19), then

$$\xi_{13} = \left(\frac{F_A}{F_C}\right)^2 \beta^2 - \frac{2F_A^2 \cos(1.4\theta - 37.3\beta^{1.8} - 5.3)}{F_C F_E \cos(20.3\beta - 10.2)} \beta + \left(\frac{F_A}{F_E \cos(20.3\beta - 10.2)}\right)^2. \quad (21)$$

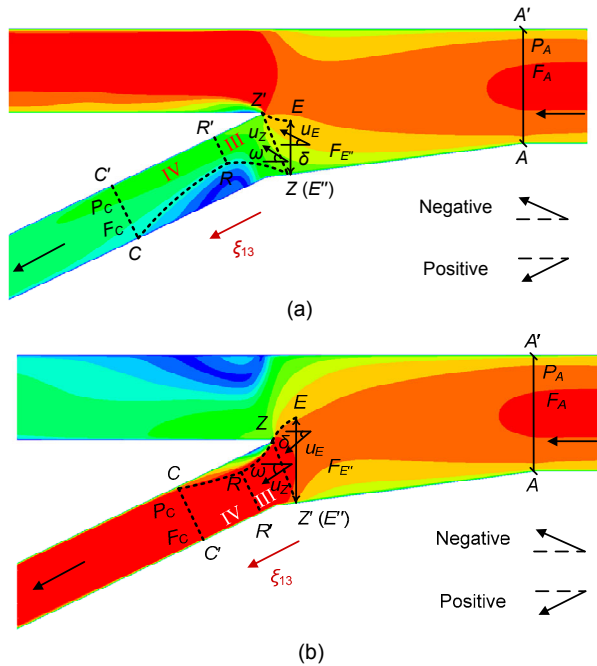


Fig. 9 Control volume used to calculate ξ_{13}
(a) $\beta=0.1$; (b) $\beta=0.9$

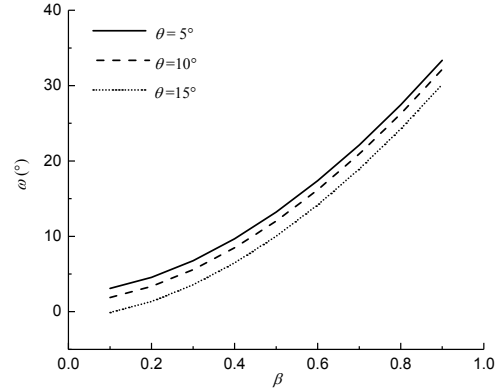


Fig. 10 Change law of ω with β at different θ

3.3 Comparison of predicted loss coefficients with measured results

The north-south direction tunnel is 4797 m long, having two one-way traffic tunnels. An off-ramp on the east line is 490 m long, and forms an angle of 12° with the mainline tunnel. An off-ramp on the west line is 485 m long, and forms an angle of 7° with the mainline tunnel. The upstream mainline, the downstream mainline and the ramp are a three-lane highway, a two-lane highway, and a one-lane highway with corresponding cross-sectional dimensions of $13.55 \text{ m} \times 7 \text{ m}$, $9.75 \text{ m} \times 7 \text{ m}$, and $7.55 \text{ m} \times 7 \text{ m}$, respectively. Field measurements were carried out on the dividing flow local loss coefficient of this tunnel. To ensure data reliability, the selected measuring cross-sections, including 1-1, 2-2, and 3-3, were at a distance of more than 20 times the hydraulic diameter from the bifurcation surface (Fig. 11). A real image of the bifurcation surface of the west line of the tunnel is shown in Fig. 12.

In the experiment, the jet fan located in the upstream mainline tunnel was regulated to ensure that the air flow was into a region of quadratic resistance law. The jet fans located in the downstream mainline tunnel and ramp were regulated to change the diversion ratio β from 0.2 to 0.8. After regulating the jet fans, it was necessary to wait a few minutes to make sure the airflow in the tunnel was in a steady state, i.e. the air velocity did not change significantly with time. Then, a Testo425 thermal anemometer (Testo AG, Germany) was used to record the air velocity data for 3 min. The average of these measurements was taken as the final air velocity at each measuring point.

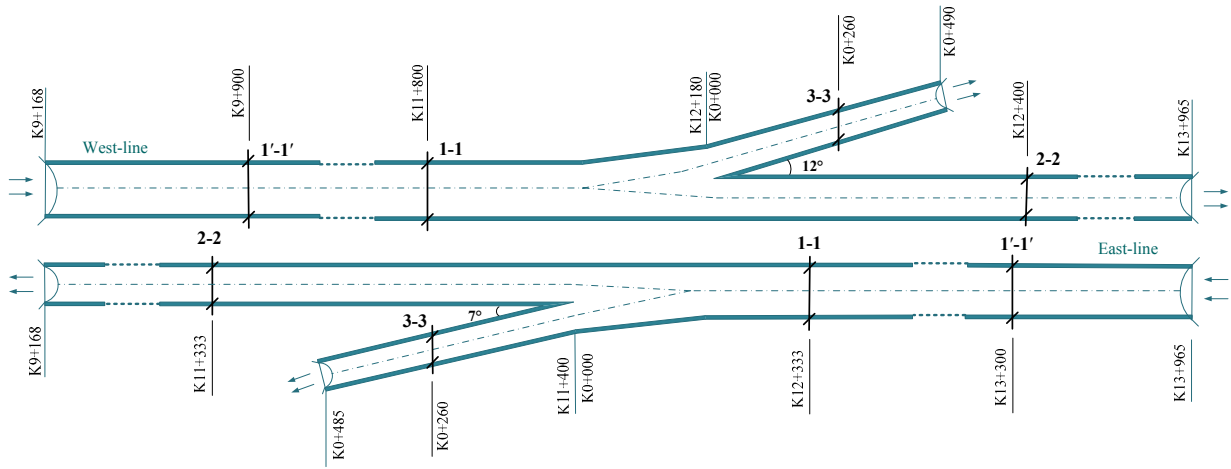


Fig. 11 Schematic diagram of the tunnel structure



Fig. 12 Bifurcation surface of the tunnel

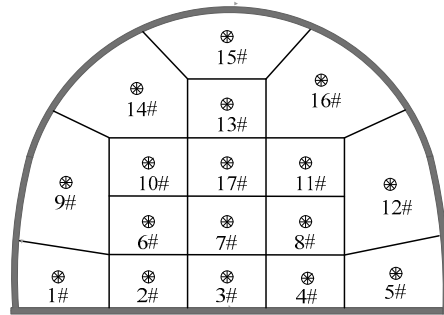


Fig. 13 Distribution of velocity measuring points

However, the air velocity of a single point on the cross-section of the tunnel cannot represent the average air velocity of the entire cross-section. Thus, several air velocity measuring points were set on the cross-section according to the fluid’s characteristics of velocity distribution on the cross-section of the tunnel, with the distribution of the serial numbers and the effective areas as shown in Fig. 13. The weighted average value of the effective areas covered by the air velocities at the measuring points was the average air velocity V of the cross-section of the tunnel. In other words, $V = \frac{\sum V_j \Delta F_j}{\sum \Delta F_j}$, where ΔF_j and V_j represent the area of each part and the air velocity of the measuring point within each area, respectively

With a pitot tube and a differential pressure gauge being connected to each other with a rubber tube, the differential pressure between the cross-sections was measured. Fig. 14 shows how a pressure test was conducted on the cross-section. Each

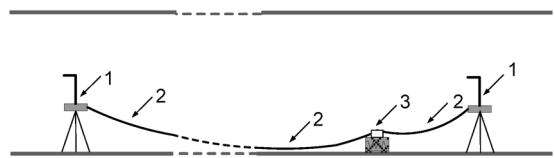


Fig. 14 Pressure tests at different cross-sections

1: pitot tube; 2: rubber tube; 3: differential pressure gauge

pressure measuring point was 2 m above the ground on the central axis of the tunnel. Since the distance between two measuring cross-sections was long, rubber tubes were placed inside the tunnel one day before the test to allow the air pressure to equilibrate. Joints of the rubber tubes were connected firmly and tightly without air leakage, and the entrance of water and other foreign bodies was prevented. Based on the measured air velocity and differential pressure, the dividing flow local loss coefficients of the tunnel, ζ_{12} and ζ_{13} , could be calculated according to the following formulas:

$$\xi_{12} = \frac{2P_{12} - 2(\Delta P_1 + 2\Delta P_2) + \rho(u_1^2 - u_2^2)}{\rho u_1^2}, \quad (22)$$

$$\xi_{13} = \frac{2P_{13} - 2(\Delta P_1 + 2\Delta P_3) + \rho(u_1^2 - u_3^2)}{\rho u_1^2}, \quad (23)$$

where the subscripts 1, 2, and 3 represent the cross-sections 1-1, 2-2, and 3-3, respectively; P_{12} is the differential pressure between cross-sections 1-1 and 2-2; P_{13} is the differential pressure between cross-sections 1-1 and 3-3. ΔP is the linear loss pressure drop between the measuring cross-section and the bifurcation surface. The expression is as follows:

$$\Delta P_i = \lambda_i L_i \rho u_i^2 / (2D_i), \quad i = 1, 2, 3, \quad (24)$$

where λ is the linear loss coefficient, D is the equivalent diameter, and the value of λ is determined by a field test. Taking the upstream mainline tunnel as an example, its λ can be obtained according to the formula $\lambda_1 = \frac{2P_{1'1}D_1}{l_{1'1}\rho u_1^2}$, based on measuring the differential pressure $P_{1'1}$ between cross-sections 1'-1' and 1-1; $l_{1'1}$ is the distance between 1'-1' and 1-1; L refers to the distance from the measuring cross-section to the bifurcation surface.

Local loss coefficients for flow division under different values of β were predicted according to the theoretical formula derived in this study, and according to the formula proposed by Bassett et al. (2001).

The prediction and test results are shown in Fig. 15. Each data point shown in Fig. 15 is the average value of the loss coefficients obtained from three tests. Obviously, as β increased, ξ_{12} and ξ_{13} calculated by measured data both showed a changing pattern of an initial decline followed by an increase. Because the cross-sectional area ratio of the downstream mainline tunnel and the ramp ϕ was equal to 1.5, when β was approximately equal to 0.38, the air flux ratio $q \approx \phi$, and thus ξ_{12} and ξ_{13} in this case were the smallest. However, the values of ξ_{12} and ξ_{13} predicted according to Bassett et al. (2001)'s formula were the smallest when β was approximately equal to 0.25 and 0.52, respectively, much different from the measured values. The value of ξ_{12} predicted according to Bassett et al. (2001)'s formula was fairly consistent

with the measured data when $\beta > 0.38$, but when $\beta < 0.38$ it showed a changing pattern of an initial decline and then a slight increase as β decreased, which is inconsistent with the changes in the measured value of ξ_{12} . When $\beta = 0.31$, the prediction error was up to 240%.

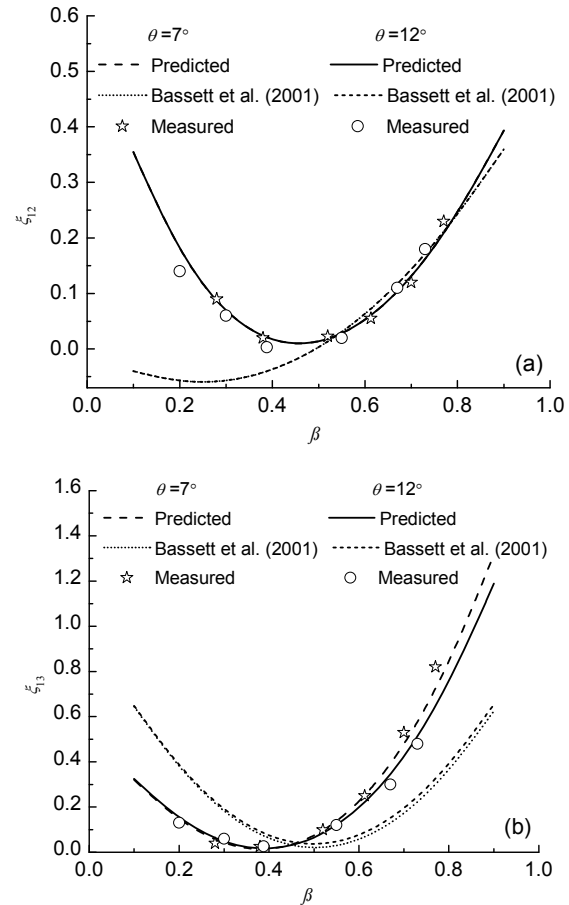


Fig. 15 Comparison of predicted loss coefficients with measured results: ξ_{12} (a); ξ_{13} (b)

In addition, as for the effect of θ on the loss coefficients, the measured results show that for the downstream mainline tunnel, the change of θ had almost no effect on ξ_{12} . For the ramp, when $\beta < 0.38$, ξ_{13} increased with increasing values of θ , and decreased with increasing values of θ . However, the value of ξ_{13} predicted according to Bassett et al. (2001)'s formula increased with increasing values of θ when $\beta > 0.38$, again inconsistent with the changes in the measured values. Obviously, Bassett et al. (2001)'s formula is not suitable for bifurcate tunnels with small bifurcation angles. However, the values of

ζ_{12} and ζ_{13} predicted according to the theoretical formula derived in this study were both in line with the measured changing patterns, with the predicted values quite consistent with the measured ones.

4 Conclusions

This paper proposes a theoretical calculation model which can effectively predict the dividing flow local loss coefficient at a tunnel bifurcation. By combining numerical simulation and theoretical derivation, the dividing flow characteristics, and local loss mechanism at a tunnel bifurcation were analyzed and a theoretical formula for calculating the dividing flow local loss coefficient in a bifurcate structure with a small angle was deduced and constructed based on the characteristics of flow separation. The following conclusions can be drawn:

1. When the diversion ratio β is small, the flow is separated on the downstream mainline tunnel sidewall close to the bifurcation point and the ramp sidewall away from the bifurcation point; when β is large, the flow is separated on the downstream mainline tunnel sidewall away from the bifurcation point and the ramp sidewall close to the bifurcation point.

2. The dividing flow local loss coefficient of the downstream mainline tunnel ζ_{12} is influenced mainly by β , while the loss coefficient of the ramp ζ_{13} is affected by both the bifurcation angles θ and β . When the air flux ratio q of the downstream mainline tunnel to the ramp is equal to their cross-sectional area ratio ϕ , ζ_{12} and ζ_{13} are at their minimum; when $q > \phi$, ζ_{12} and ζ_{13} decrease with increasing β , but ζ_{13} increases with increasing θ . When $q < \phi$, ζ_{12} and ζ_{13} increase with increasing β , but ζ_{13} declines with increasing θ .

3. A theoretical formula which can be used to predict the dividing flow local loss coefficient of a bifurcate tunnel is established based on an airflow deflection angle assumption. Compared to existing formulas, the proposed formula has a higher precision in prediction.

4. Note that the expanding section (cross-section area variation near the split) exists to avoid traffic jams near the tunnel bifurcation. The effects of the structural form and parameters (e.g. the length and form of the change in cross-sectional area) of the expanding section on loss coefficients cannot be ig-

nored. More in-depth research and further discussion of this will be conducted in the future.

References

- Abdulwahhab M, Injeti NK, Dakhi SF, 2013. Numerical prediction of pressure loss of fluid in a T-junction. *International Journal of Energy and Environment*, 4(2):253-264.
- Bassett MD, Winterbone DE, Pearson RJ, 2001. Calculation of steady flow pressure loss coefficients for pipe junctions. *Proceedings of the Institution of Mechanical Engineers, Part C: Journal of Mechanical Engineering Science*, 215(8):861-881.
<https://doi.org/10.1177/095440620121500801>
- Costa NP, Maia R, Proenca MF, et al., 2006. Edge effects on the flow characteristics in a 90deg tee junction. *Journal of Fluids Engineering*, 128(6):1204-1217.
<https://doi.org/10.1115/1.2354524>
- Du T, Yang D, Peng SN, et al., 2015. A method for design of smoke control of urban traffic link tunnel (UTLT) using longitudinal ventilation. *Tunnelling and Underground Space Technology*, 48:35-42.
<https://doi.org/10.1016/j.tust.2015.02.001>
- Ghostine R, Vazquez J, Terfous A, et al., 2013. A comparative study of 1D and 2D approaches for simulating flows at right angled dividing junctions. *Applied Mathematics and Computation*, 219(10):5070-5082
<https://doi.org/10.1016/j.amc.2012.11.048>
- Hager WH, 1984. An approximate treatment of flow in branches and bends. *Proceedings of the Institution of Mechanical Engineers, Part C: Journal of Mechanical Engineering Science*, 198(4):63-69.
https://doi.org/10.1243/PIME_PROC_1984_198_088_02
- Hager WH, 2010. Losses in flow. *Wastewater Hydraulics: Theory and Practice*. Springer, Berlin, Heidelberg, p.17-54.
https://doi.org/10.1007/978-3-642-11383-3_2
- Hong SW, Exadaktylos V, Lee IB, et al., 2017. Validation of an open source CFD code to simulate natural ventilation for agricultural buildings. *Computers and Electronics in Agriculture*, 138:80-91.
<https://doi.org/10.1016/j.compag.2017.03.022>
- Idelchik IE, Steinberg MO, Malyavskaya GR, et al., 2008. *Handbook of Hydraulic Resistance*. Laurier Books Ltd., New York, USA, p.413-501.
- Itō H, Imai K, 1973. Energy losses at 90° pipe junctions. *Journal of the Hydraulics Division*, 99(9):1353-1368.
- Iwanami S, Tetsuo S, Hiroshi K, 2008. Study on flow characteristics in right-angled pipe fittings: 1st report, on case of water flow. *Transactions of the Japan Society of Mechanical Engineers*, 35(269): 97-106.
- Li JM, Liu SS, Li YF, et al., 2012. Experimental study of smoke spread in titled urban traffic tunnels fires. *Procedia Engineering*, 45:690-694.
<https://doi.org/10.1016/j.proeng.2012.08.224>
- Li L, Li YL, Huang JT, et al., 2001. Numerical simulation and

- experimental study on water flow in Y-type tube. *Journal of Hydraulic Engineering*, (3):49-53 (in Chinese).
<https://doi.org/10.3321/j.issn:0559-9350.2001.03.010>
- Li Q, Chen C, Deng YW, et al., 2015. Influence of traffic force on pollutant dispersion of CO, NO and particle matter (PM_{2.5}) measured in an urban tunnel in Changsha, China. *Tunnelling and Underground Space Technology*, 49:400-407.
<https://doi.org/10.1016/j.tust.2015.04.019>
- Liao L, Yan L, Huang W, et al., 2018. Mode transition process in a typical strut-based scramjet combustor based on a parametric study. *Journal of Zhejiang University-SCIENCE A (Applied Physics & Engineering)*, 19(6):431-451.
<https://doi.org/10.1631/jzus.A1700617>
- Lin GH, Ferng YM, 2016. Investigating thermal mixing and reverse flow characteristics in a T-junction using CFD methodology. *Applied Thermal Engineering*, 102:733-741.
<https://doi.org/10.1016/j.applthermaleng.2016.03.124>
- Lukiyanto YB, Wardana ING, Wijayanti W, et al., 2016. Secondary flow behaviour in various rounded-edge bifurcation T-Junctions and its relation to head loss. *International Journal of Fluid Mechanics Research*, 43(3): 206-217.
<https://doi.org/10.1615/InterJFluidMechRes.v43.i3.20>
- Mangani L, Buchmayr M, Darwish M, 2014. Development of a novel fully coupled solver in OpenFOAM: steady-state incompressible turbulent flows. *Numerical Heat Transfer, Part B: Fundamentals*, 66(1):1-20.
<https://doi.org/10.1080/10407790.2014.894448>
- Matthew GD, 1975. Simple approximate treatments of certain incompressible duct flow problems involving separation. *Journal of Mechanical Engineering Science*, 17(2):57-64.
https://doi.org/10.1243/JMES_JOUR_1975_017_011_02
- McKeon BJ, Li J, Jiang W, et al., 2004. Further observations on the mean velocity distribution in fully developed pipe flow. *Journal of Fluid Mechanics*, 501:135-147.
<https://doi.org/10.1017/S0022112003007304>
- Meng Q, Qu XB, Wang XC, et al., 2011. Quantitative risk assessment modeling for nonhomogeneous urban road tunnels. *Risk Analysis*, 31(3):382-403.
<https://doi.org/10.1111/j.1539-6924.2010.01503.x>
- Mignot E, Zeng C, Dominguez G, et al., 2013. Impact of topographic obstacles on the discharge distribution in open-channel bifurcations. *Journal of Hydrology*, 494: 10-19.
<https://doi.org/10.1016/j.jhydrol.2013.04.023>
- Miller DS, 1971. Internal Flow: a Guide to Losses in Pipe and Duct Systems. British Hydromechanics Research Association, Cranfield, UK, p.303-360.
- Mohamed MS, Larue JC, 1990. The decay power law in grid-generated turbulence. *Journal of Fluid Mechanics*, 219:195-214.
<https://doi.org/10.1017/S0022112090002919>
- Momplot A, Kouyi GL, Mignot E, et al., 2017. Typology of the flow structures in dividing open channel flows. *Journal of Hydraulic Research*, 55(1):63-71.
<https://doi.org/10.1080/00221686.2016.1212409>
- MOT (Ministry of Transport of the People's Republic of China), 2018. Design Specification for Highway Alignment, JTG D20-2017. MOT (in Chinese).
- Nan CZ, Ma JM, Luo Z, et al., 2015. Numerical study on the mean velocity distribution law of air backflow and the effective interaction length of airflow in forced ventilated tunnels. *Tunnelling and Underground Space Technology*, 46:104-110.
<https://doi.org/10.1016/j.tust.2014.11.006>
- Nazif HR, Tabrizi HB, 2011. Comparison of standard turbulent wall function with a non-equilibrium wall model. *International Journal of Fluid Mechanics Research*, 38(6):499-508.
<https://doi.org/10.1615/InterJFluidMechRes.v38.i6.30>
- Oka K, Itō H, 2005. Energy losses at tees with large area ratios. *Journal of Fluids Engineering*, 127(1):110-116.
<https://doi.org/10.1115/1.1852475>
- Reynolds O, 1895. On the dynamical theory of incompressible viscous fluids and the determination of the criterion. *Philosophical Transactions of the Royal Society of London. A*, 186:123-164.
<https://doi.org/10.1098/rsta.1895.0004>
- Shi X, Lü HX, Zhu DL, et al., 2013. Flow resistance and characteristics of PVC tee pipes. *Transactions of the Chinese Society for Agricultural Machinery*, 44(1):73-79 (in Chinese).
<https://doi.org/10.6041/j.issn.1000-1298.2013.01.015>
- Shih TH, Zhu J, Lumley JL, 1994. A new Reynolds stress algebraic equation model. *Computer Methods in Applied Mechanics and Engineering*, 125(1-4):287-302.
[https://doi.org/10.1016/0045-7825\(95\)00796-4](https://doi.org/10.1016/0045-7825(95)00796-4)
- Shih TH, Liou WW, Shabbir A, et al., 1995. A new $k-\epsilon$ eddy viscosity model for high Reynolds number turbulent flows. *Computers & Fluids*, 24(3):227-238.
[https://doi.org/10.1016/0045-7930\(94\)00032-T](https://doi.org/10.1016/0045-7930(94)00032-T)
- Song Y, Li XB, Wang SH, et al., 2016. Experimental study on determination and correction method of wind speed in wind station of rectangular roadway based on LDA. *Journal of Safety Science and Technology*, 12(1):169-175 (in Chinese).
<https://doi.org/10.11731/j.issn.1673-193x.2016.01.032>
- Tan Z, Gao HO, 2015. Traffic control for air quality management and congestion mitigation in complex urban vehicular tunnels. *Transportation Research Part C: Emerging Technologies*, 58:13-28.
<https://doi.org/10.1016/j.trc.2015.06.004>
- Tavoularis S, Corrsin S, 1981. Experiments in nearly homogeneous turbulent shear flow with a uniform mean temperature gradient. Part 2. The fine structure. *Journal of Fluid Mechanics*, 104:349-367.
<https://doi.org/10.1017/S0022112081002942>
- Versteeg HK, Malalasekera W, 1995. An Introduction to Computational Fluid Dynamics: the Finite Volume

Method. Longman Scientific & Technical, New York, USA, p.66-69.

Wu K, Huang ZY, Zhang JS, et al., 2017. An Urban Tunnel Ventilation Test Device with a Ramp. CN Patent 104564122B (in Chinese).

中文概要

题目: 小夹角分叉隧道分流局部损失模型

目的: 掌握分叉隧道的空气流动特征与阻力损失特性是进行分叉隧道通风设计和控制的关键。本文旨在探讨小角度分叉结构中的流动特征及局部损失机制,并基于流动分离机制构建可供设计使用的分叉隧道分流局部损失系数的理论公式。

创新点: 1. 揭示气流在小角度分叉结构中的流动分离特征及损失机制; 2. 提出流向偏转角假设,建立可供设计使用的分叉隧道分流局部损失预测模型。

方法: 1. 通过数值模拟,获得隧道分叉处的流动特征(图 5、6a 和 6d),以及分流局部损失系数随分流比及

夹角的变化规律(图 6b 和 6c); 2. 通过理论推导,构建小夹角分叉结构的分流局部损失系数预测公式(公式(18)和(21)); 3. 通过现场实测,验证预测公式的可靠性(图 15)。

结论: 1. 空气在隧道分叉处的分流将导致流速和流向的变化; 当分流比 β 较小时,流动分离出现在靠近分叉点一侧的主线边壁和远离分叉点一侧的匝道边壁; 当 β 较大时,流动分离出现在远离分叉点一侧的主线边壁和靠近分叉点一侧的匝道边壁。2. 当分流后主线与匝道的流量比 q 等于两者的面积比 ϕ 时,主线及匝道的分流局部损失系数 ζ_{12} 和 ζ_{13} 最小; 当 $q > \phi$ 时, ζ_{12} 和 ζ_{13} 均随 β 的增大而减小,且 ζ_{13} 随着 θ 的增大而增大; 当 $q < \phi$ 时, ζ_{12} 和 ζ_{13} 均随 β 的增大而增大,且 ζ_{13} 随着 θ 的增大而减小。3. 基于隧道分叉处的流动分离机制,提出了空气流向偏转角假设,构建了可用于预测分叉隧道分流局部损失系数的理论公式,与已有文献公式相比,具有更好的预测精度。

关键词: 分叉隧道; 分流; 局部损失机制; 流动分离特征; 计算流体动力学; 理论公式